发光学报
CHINESE JOURNAL OF LUMINESCENCE
中文核心期刊
主管：中国科学院
主办：中国科学院长春光学精密机械与物理研究所
中国物理学会发光分会
主编：申德振

用于固态照明的Mn^{4+}离子光谱学

BRIK Mikhail G, 马崇庚, SRIVASTAVA Alok M, PIASECKI Michal

引用本文:
BRIK Mikhail G, 马崇庚, SRIVASTAVA Alok M, 等. 用于固态照明的Mn^{4+}离子光谱学[J]. 发光学报, 2020, 41(9): 1011-1029.
BRIK Mikhail G, MA Chong-geng, SRIVASTAVA Alok M, et al. Mn^{4+} Ions for Solid State Lighting[J]. *Chinese Journal of Luminescence*, 2020, 41(9): 1011-1029.

在线阅读 View online: https://doi.org/10.37188/fgxb20204109.1011

Article ID: 1000-7032(2020)09-1011-19

Mn^{4+} Ions for Solid State Lighting

BRIK Mikhail G[1,2,3*], MA Chong-geng[1],
SRIVASTAVA Alok M[4], PIASECKI Michal[3,5]

(1. *College of Sciences & CQUPT-BUL Innovation Institute, Chongqing University of Posts and Telecommunications, Chongqing* 400065, *China*;
2. *Institute of Physics, University of Tartu, Tartu* 50411, *Estonia*;
3. *Institute of Physics, Jan Długosz University, PL*-42200 *Częstochowa, Poland*;
4. *Consultant to GE Current, A Daintree Company, Ohio* 44110, *USA*;
5. *Department of Solid State Physics, Eastern European National University, Lutsk* 43025, *Ukraine*)

* *Corresponding Author, E-mail: mikhail. brik@ ut. ee*

Abstract: Phosphors activated with Mn^{4+} ion are gaining prominence in the field of solid-state lighting as generators of red photon. In the present review, we focus on several important points that are fundamentally important to produce a commercially useful phosphor. This includes an understanding of the Mn^{4+} energy levels in the free state and in the crystal fields and of the host dependent variations in the Mn^{4+} emission wavelength. Additionally, we formulate several practical recommendations on how to tune the emission wavelength and emission intensity of Mn^{4+}-doped phosphors. The main spectroscopic parameters of the Mn^{4+} ion in more than 100 phosphor materials are collected and discussed.

Key words: Mn^{4+} ions; red phosphors; white LED
CLC number: O482.31 **Document code**: A **DOI**: 10.37188/fgxb20204109.1011

用于固态照明的 Mn^{4+} 离子光谱学

BRIK Mikhail G[1,2,3*], 马崇庚[1], SRIVASTAVA Alok M[4], PIASECKI Michal[3,5]

(1. 重庆邮电大学 理学院 &“重庆邮电大学-伦敦布鲁内尔大学”交叉创新研究院, 重庆 400065;
2. 塔尔图大学 物理所, 爱沙尼亚 塔尔图 50411; 3. 琴斯托霍瓦师范大学 物理所, 波兰 琴斯托霍瓦 42200;
4. 戴恩特里公司通用电气顾问部, 美国 克利夫兰 44110; 5. 东欧国立大学 固态物理系, 乌克兰 卢茨克 43025)

摘要: Mn^{4+} 离子激活的荧光粉在固态照明领域作为红光发射的热点载体正日益受到关注。我们针对当前研究热度撰写了 Mn^{4+} 离子光谱学的回顾,并在回顾中聚焦了许多对红色荧光粉商业研制有价值的重要基础研究点。这些研究点涵盖了如何理解自由和晶场状态下 Mn^{4+} 离子的能级结构以及 Mn^{4+} 发射波长对基质的依赖关系。此外,我们就如何实验调控 Mn^{4+} 离子掺杂型荧光粉的发射波长和发光强度给出了许多实际可行的建议。更为重要的是,我们收集并讨论了 100 多种荧光粉基质中 Mn^{4+} 离子光谱学参数,对它们的理解将会为未来 Mn^{4+} 掺杂型红色荧光粉的实验开发奠定基础。

关 键 词: Mn^{4+} 离子; 红色荧光粉; 白光 LED

收稿日期: 2020-07-03; **修订日期**: 2020-07-12
基金项目: 重庆市留学归国人员创新与创业支持计划(CX2019055); 重庆邮电大学外国专家支持计划(W2017011); 爱沙尼亚研究委员会基金(PUT PRG111); 欧洲区域发展基金(TK141); 波兰国家科学中心计划(2018/31/B/ST4/00924)资助项目
Supported by Chongqing Innovation and Entrepreneurship Programs for Returned Overseas Chinese Scholars(CX2019055); Programme for the Foreign Expertsoffered by CQUPT(W2017011); Estonian Research Council grant(PUT PRG111); European Regional Development Fund(TK141); NCN Project(2018/31/B/ST4/00924)

1 Introduction

1.1 Review Outline

The phosphor converted LEDs are gaining commercial importance in general and specialty lighting because of their higher efficiency and longer lifetime relative to fluorescent lighting. Active research in this field is being performed in many industrial and academic research groups worldwide[1-14] and references therein. Numerous phosphor materials based on different crystalline solids have been developed so far. One common feature of all these phosphors is that their performance relies on additionally introduced impurities (dopants), which after absorption of a properly chosen excitation radiation can emit light in a certain spectral range. The transition metal and rare-earth ions are those widely used impurities. Their unfilled d- and f-electron shells are characterized by a large number of electronic states, which can be split by crystal field[15], thus giving rise to a variety of the absorption and emission transitions in different spectra ranges.

In the present review, we summarize the most important information related to the Mn^{4+} ions (their electronic structure, energy levels, crystal field effects) and crystalline solids doped with these ions for applications as the red phosphors for white LEDs. We start with the properties of the $3d^3$ electron configuration, introduce the main spectroscopic parameters that are needed to describe the optical spectra of these materials, give a list of more than 100 phosphor materials doped with the Mn^{4+} ions with a description of the overall trend that related the emission spectra to the nephelauxetic effect. Very important questions of tunability of the Mn^{4+} emission peak position and emission intensity are also addressed. Finally, we explain several misconceptions about the Mn^{4+} spectra in crystalline solids.

1.2 Basic Properties of Considered d^3 Electron Configuration

In this review paper, we focus our attention on some representatives of the transition metal group with unfilled 3d electron shell. Comprehensive reviews of crystal field properties of the entire series of $3d^n$ ions series were published earlier[16]. In this paper, attention is focused on ions with $3d^3$ electron configuration. These ions are V^{2+}, Cr^{3+}, Mn^{4+}, Fe^{5+}, where Cr^{3+} and Mn^{4+} are widely used for the solid-state lighting due to their energy level structures that is optimum for the required excitation and emission wavelengths.

Deep understanding of the optical properties of these impurities in solids and functionality features of the corresponding phosphors bearing these impurities is possible only if a clear picture of the origin of all electronic states and their interaction with the crystalline environment is formed. Recently[17], we published a detailed tutorial review on the electronic properties of the d^3 electron configuration. Here we remind the reader of the salient points that should be kept in mind when working with such ions and which will be frequently used in this review:

(1) There are five 3d orbitals, which have the same principal quantum number $n = 3$ and orbital quantum number $l = 2$, but differ by the magnetic quantum numbers $m_l = -2, -1, 0, 1, 2$.

(2) Each orbital can accommodate not more than two electrons, whose spin momenta in such a case should be opposite, as is stated by the Pauli exclusion principle. This gives $5 \times 2 = 10$ single-electron states in total. There are 120 ways (different permutations) to distribute three electrons through these single electron states that is calculated as follows: $10!/(3! \times (10-3)!) = 120$.

(3) The total wave functions of such configuration are antisymmetric linear combinations of products of three single electron wave functions built following the quantum-mechanical rules of the orbital momenta addition. Thorough consideration of all 120 microstates reveals that they are grouped in a way to give rise to eight highly degenerated terms with different values of the total orbital momentum $\boldsymbol{L}$ and total spin momentum $\boldsymbol{S}$.

(4) These terms are as follows (in the $^{2S+1}\boldsymbol{L}$ notation): ^4F (the ground term as specified by the Hund's rule), ^4P, ^2P, $^2D_{(1)}$, $^2D_{(2)}$, ^2F, ^2G, ^2H. Here the superscripts "4" and "2" denote the spin-quartet states ($S = 3/2$) and the spin-doublet states

($S=1/2$), respectively. The letters P, D, F, G, H stand for the values of $L=1, 2, 3, 4, 5$, correspondingly. The subscripts "(1)" and "(2)" distinguish between two ^2D terms. The degeneracy degree of each term is found as $(2S+1)\times(2L+1)$.

(5) Coulomb interaction between the 3d electrons makes these terms to have different energy, which-after careful calculations-can be expressed as simple combinations of the so-called Racah parameters B and C as follows: $^4F(0)$, $^4P(15B)$, $^2P(9B+3C)$, $^2D_{(1)}(20B+5C+\sqrt{193B^2+8BC+4C^2})$, $^2D_{(2)}(20B+5C-\sqrt{193B^2+8BC+4C^2})$, $^2F(24B+3C)$, $^2G(4B+3C)$, $^2H(9B+3C)$. The energies of the ^2P and ^2H terms are equal by coincidence. Typical values of the Racah parameters B and C for the $3d^3$ ions in a free state are given in Tab. 1[18].

Tab. 1　Free ion values (in cm^{-1}) of the Racah parameters for some $3d^3$ ions

Ion	B	C
V^{2+}	766	2 855
Cr^{3+}	918	3 850
Mn^{4+}	1 160	4 303
Fe^{5+}	1 210	5 066

(6) Free ions' *LS* terms are split into a number of states in a crystal field. The splitting patterns depend on the crystal field symmetry and can be obtained by using group theory. In the cubic crystal field, all possible split states are listed in Tab. 2. Orbital singlet, doublet, triplet states are denoted by letters A, E, T, correspondingly, which also stand for the irreducible representations of the O_h point group.

In the crystal fields of lower symmetries further reduction of the degree of degeneracy can be possible, until all states become orbital singlets.

Tab. 2　Splitting of the S, P, D, G, G, H terms in the cubic crystal field

Terms	Split states
S ($L=0$)	A_1
P ($L=1$)	T_1
D ($L=2$)	$E+T_2$
F ($L=3$)	$A_2+T_1+T_2$
G ($L=4$)	$A_1+E+T_1+T_2$
H ($L=5$)	$E+T_1+T_1+T_2$

(7) Three interactions are mainly responsible for the formation of energy levels of the d ions in solids. In the order of the decreasing magnitude they are as follows: (ⅰ) the Coulomb interaction between electrons in the unfilled d shell, which produces the *LS* terms of free ions; (ⅱ) the crystal field splitting of the free ion's *LS* terms, and (ⅲ) spin-orbit interaction, which produces the fine structure of the split crystal field levels.

(8) Quantitative calculations of the crystal field splittings are possible within the crystal field theory. The Tanabe-Sugano diagrams show variation of the split energy levels depending on the crystal field strength denoted by Dq. In these diagrams, the energy of the ground state is always taken as zero; the crystal field symmetry is cubic (which corresponds either to the octahedral or tetrahedral coordination of the impurity ions). The horizontal axis is the Dq/B ratio, the vertical axis is the E/B ratio, where E is the energy of a particular state, and B is the Racah parameter. For the d^3 ions in the octahedral environment the separation between the $^4A_2$ and $^4T_2$ states is equal to $10Dq$. All notations in Fig. 1 come from Tab. 2.

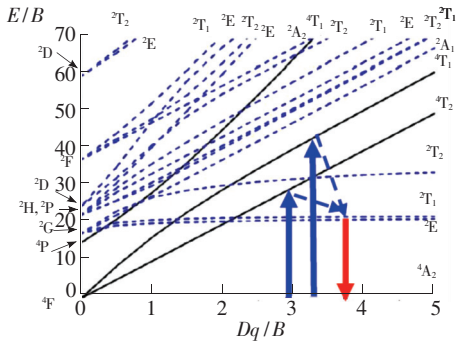

Fig. 1　Tanabe-Sugano diagram for the d^3 electron configuration in the octahedral crystal field. $C/B=4.5$. The spin-quartet and spin-doublet states are shown by the solid and dashed lines, respectively.

(9) It is important to note that at the value of $Dq/B\approx 2$ there is a change of the first excited state. When $Dq/B>2$, the absorption spectra are dominated by two broad spin-allowed transitions $^4A_2\rightarrow{}^4T_2$ and $^4A_2\rightarrow{}^4T_1$ (blue upward arrows in Fig. 1). After non-radiative relaxation shown by the dashed arrows,

sharp spin-forbidden transition ascribed to the $^2E \rightarrow {}^4A_2$ transition (red downward arrow) takes place. If $Dq/B < 2$, the absorption spectra are still formed by the same above-listed transitions, but in the emission spectra a broad band appears, which is due to the $^4T_2 \rightarrow {}^4A_2$ transition. In the vicinity of the point of intersection of the ^2E and $^4T_2$ states both types of the emission transition occur, which can give rise to interesting phenomena discussed below.

(10) The Dq, B and C parameters can be easily evaluated from the d^3 ions experimental spectra, using the energies $E(^4T_2)$, $E(^4T_1(^4F))$ and $E(^2E)$ of the $^4T_2$, $^4T_1(^4F)$ and ^2E states:

$$E(^4T_2) = 10Dq, \tag{1}$$

$$\frac{B}{Dq} = \frac{\left(\frac{\Delta E}{Dq}\right)^2 - 10\left(\frac{\Delta E}{Dq}\right)}{15\left(\frac{\Delta E}{Dq} - 8\right)}, \tag{2}$$

$$\frac{E(^2E)}{B} = \frac{3.05C}{B} + 7.90 - \frac{1.80B}{Dq}, \tag{3}$$

where $\Delta E = E(^4T_1(^4F)) - E(^4T_2)$[19].

This information presented in the form of the bullet points creates the minimal necessary background for the discussion, clarification and explanation of the main spectroscopic properties of the Cr^{3+} and Mn^{4+} ions doped phosphors.

2 Mn^{4+} Ions for White LEDs

2.1 General Concepts

Discovery of blue light emitting diodes (LED) based on GaN or InGaN[20-21] allowed to produce bright, efficient and durable sources of white light. The first white LEDs were based on GaN blue LED chip emitting at 450 nm combined with the yellow phosphor $Y_3Al_5O_{12}:Ce^{3+}$ (Fig. 2). The latter partially absorbs blue light and converts it into broad yellow emission that is due to the Ce^{3+} 5d-4f transition. This emission when blended with the blue light of LED produces white light.

The main parameters that characterize white LEDs are the color correlated temperature (CCT) and the color rendering index (CRI). The CCT is the temperature of the ideal black body radiator that emits light with the spectral distribution approximating a given white LED spectrum in the best way. The higher CCT values (5 000 – 6 000 K) are characteristic of somewhat "bluish" white light, which is called "cold white light". The lower CCT values (3 000 – 4 000 K) correspond to the "yellowish", or "warm white light". The warm white light LEDs are more popular for living interiors, while the cold white light LEDs are more often used for the office spaces. The CRI indicates ability of the light source to reproduce true or natural colors of the objects. By definition, the sun light has the highest CRI of 100.

However, due to the lack of red emission in the original white LEDs spectra (compare the relative intensities of the blue, yellow, and red emissions in Fig. 2), the white light generated has rather low CRI (~76) and rather high color correlated temperature (~6 200 K)[10], and is perceived by the human eye as the "cold" white light.

Addition of some red phosphor to such white LED would significantly improve the white light characteristics. One of the best red phosphors, which has already found numerous commercial applications, is $K_2SiF_6:Mn^{4+}$[22-27]. Recently, a large number of other Mn^{4+}-doped hosts have been reported, many of them are listed in Refs. [14,28-30].

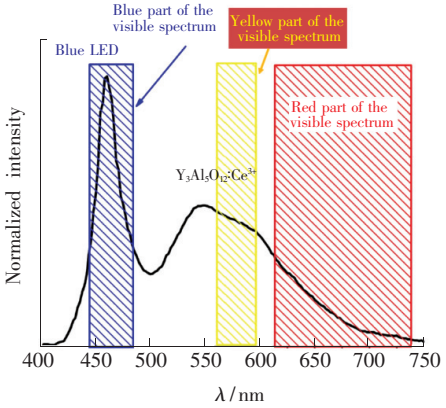

Fig. 2 Emission spectrum of a white LED based on the InGaN blue LED and $Y_3Al_5O_{12}:Ce^{3+}$ yellow phosphor

Why are the Mn^{4+}-doped phosphors so attractive? Some reasons are listed here:

(1) Mn is cheaper than the rare-earth activators, therefore, the cost of the LEDs mass production with the Mn^{4+}-based red phosphors can be significantly reduced if compared with the rare-earth

ions based phosphors.

(2) The energies of the Mn^{4+} $^4A_2 \rightarrow {}^4T_2$ and $^4A_2 \rightarrow {}^4T_1$ transitions correspond to the blue light (~450 nm) and ultraviolet (UV) light (~330 – 380 nm). This allows to use the blue and UV LEDs as the direct excitation sources for this activator.

(3) Due to the direct excitation to the Mn^{4+} states, the energy losses are minimized (if the impurity is excited by the energy transfer from the host after over-band-gap excitation, efficiency of such energy transfer is the crucial factor).

(4) Mn^{4+} ions are always described by the strong crystal field case, *i. e.* emission is always due to the sharp spin-forbidden $^2E \rightarrow {}^4A_2$ transition.

(5) The emission energies of the $^2E \rightarrow {}^4A_2$ transition can be tuned in a very wide range, from ~620 nm to ~720 nm[7], by changing the crystalline host, which opens numerous possibilities for tuning emission color from red to deep-red.

(6) The $^2E \rightarrow {}^4A_2$ emission is very sharp, with the full width at the half maximum of a few nm only, which ensures color purity—a very important parameter for the display applications.

(7) Plenty of host materials can accommodate the Mn^{4+} ions, and with partial cation and/or anion substitution the tunability of the Mn^{4+} red emission is greatly enhanced.

2.2 Host Materials

All host materials that can be doped with the Mn^{4+} ions can conditionally be divided into three groups: oxides, fluorides and oxyfluorides. This classification may not be necessarily correct from the pure chemical point of view. It is based rather on the type of ligands surrounding impurity, which can be either oxygen or fluorine anions. An interesting intermediate case of oxyfluorides is also existing, but the number of such compounds is not yet as large as the number of the conventional oxide or fluoride phosphors.

Tab. 3 – 5 list a large number of solids (divided into the groups conditionally referred to as fluorides, oxides, oxyfluorides) doped with the Mn^{4+} ions that have been reported in recent publications. The values of the crystal field strength *Dq*, Racah parameters *B* and *C* and the energetic position of the emitting ^2E energy level are all given.

Tab. 3　Spectroscopic parameters of Mn^{4+} ions in fluoride phosphors. *Dq* is the crystal field splitting, *B* and *C* are the Racah parameters, $E(^2E)$ is the ZPL position, all these values are in cm^{-1}

Host	*Dq*	*B*	*C*	$E(^2E)$	Ref.	Host	*Dq*	*B*	*C*	$E(^2E)$	Ref.
$BaGeF_6$	2 128	609	3 785	16 038	[31]	K_2GeF_6	2 123	593	3 824	16 050	[47]
$BaSiF_6$	2 141	568	3 879	16 050	[32]	K_2GeF_6	2 150	590	3 831	16 050	[48]
$BaSnF_6$	2 141	529	3 996	16 129	[33]	K_2LiAlF_6	2 150	574	3 849	16 000	[49]
$BaTiF_6$	2 128	609	3 789	16 050	[34]	K_2LiGaF_6	2 150	582	3 847	16 051	[50]
Cs_2BAlF_6 (B = K, Rb)	2 174	557	3 930	16 129	[35]	K_2MnF_6	2 183	604	3 821	16 129	[51]
Cs_2GeF_6	2 200	480	4 074	16 028	[36]	K_2NaAlF_6	2 165	600	3 815	16 078	[52]
Cs_2HfF_6	2 006	601	3 825	16 093	[37]	K_2NaGaF_6	2 133	595	3 837	16 104	[53]
Cs_2MnF_6	2 136	534	3 942	16 000	[38]	K_2NaScF_6	2 134	541	3 950	16 077	[54]
Cs_2NaScF_6	2 105	568	3 874	16 026	[39]	K_2NaScF_6	2 132	562	3 929	16 155	[39]
Cs_2SiF_6	2 174	557	3 895	16 021	[40]	K_2NbF_7	2 141	521	4 013	16 129	[55]
Cs_2SnF_6	2 101	589	3 830	16 042	[41]	K_2SiF_6	2 390	770	3 435	16 100	[48]
Cs_2ZrF_6	2 105	601	3 816	16 077	[42]	K_2SiF_6	2 200	605	3 806	16 091	[56]
Cs_3AlF_6	2 141	585	3 834	16 025	[43]	K_2SiF_6	2 197	599	3 750	15 873	[57]
$KNaMF_7$ (M = Nb, Ta)	2 105	635	3 757	16 129	[44]	K_2TaF_7	2 166	551	3 955	16 160	[58]
$KTeF_5$	2 174	557	3 930	16 120	[45]	K_2TiF_6	2 105	635	3 714	16 000	[59]
$KZnF_3$	2 105	607	3 785	16 026	[46]	$K_2TiF_6 \cdot BaF(HF_2)$	2 160	540	3 995	16 207	[60]

Tab. 3 (Continue)

Host	*Dq*	*B*	*C*	*E*(^{2}E)	Ref.	Host	*Dq*	*B*	*C*	*E*(^{2}E)	Ref.
K_3GaF_6	2 141	619	3 808	16 181	[61]	Na_2TiF_6	2 092	554	3 940	16 207	[75]
K_3ScF_6	2 128	551	3 918	16 051	[62]	Na_3AlF_6	2 151	617	3 795	16 129	[76]
K_3ZrF_7	2 128	584	3 871	16 129	[63]	Na_3GaF_6	2 151	600	3 791	16 000	[77]
$LiSrAlF_6$	2 151	504	4 070	16 181	[64]	Na_3HTiF_8	2 161	645	3 736	16 140	[78]
$LiSrGaF_6$	2 141	455	4 183	16 181	[65]	Rb_2CsSiF_7	2 222	588	3 815	16 000	[79]
$Li_{0.5}Na_{1.5}SiF_6$	2 128	455	4 167	16 129	[66]	Rb_2GeF_6	2 153	570	3 886	16 078	[80]
$Li_3Na_3Al_2F_{12}$	2 141	536	3 902	15 898	[67]	Rb_2KAlF_6	2 174	557	3 930	16 129	[35]
$Li_3Na_3Ga_2F_{12}$	2 146	548	3 964	15 923	[68]	Rb_2MF_6 (M = Ti, Zr)	2 105	635	3 757	16 129	[81]
$(NH_4)_2NaInF_6$	2 128	536	3 938	16 000	[69]	Rb_2NaScF_6	2 174	565	3 902	16 103	[39]
$(NH_4)_2NaScF_6$	2 110	571	3 882	16 077	[70]	Rb_2SnF_6	2 137	573	3 894	16 129	[82]
$(NH_4)_3AlF_6$	2 132	562	4 006	16 393	[71]	Rb_3AlF_6	2 141	593	3 866	16 181	[83]
$NaKSiF_6$	2 222	588	3 857	16 129	[72]	Rb_3SiF_7	2 222	588	3 823	16 026	[84]
Na_2GeF_6	2 174	557	3 956	16 207	[73]	$ZnSiF_6 \cdot 6H_2O$	2 174	590	3 779	15 898	[85]
Na_2SiF_6	2 174	775	3 475	16 207	[74]	$ZnSiF_6 \cdot 6H_2O$	2 174	557	3 846	15 873	[86]
Na_2SnF_6	2 101	589	3 873	16 171	[41]	$ZnTiF_6 \cdot 6H_2O$	2 141	568	4 031	16 129	[87]

Tab. 4 Spectroscopic parameters of Mn^{4+} ions in oxide phosphors, all notations are the same as in Tab. 3, the hosts with questionable Racah parameters *B* and *C* are highlighted

Host	*Dq*	*B*	*C*	*E*(^{2}E)	Ref.	Host	*Dq*	*B*	*C*	*E*(^{2}E)	Ref.
Al_2O_3 *	2 170	900	2 800	14 950 14 866	[88]	Gd_2MgTiO_6	2 066	997	2 514	14 685	[106]
						$LaAlO_3$	2 123	695	2 941	14 034	[107]
$BaLaZnTaO_6$	1 980	660	3 138	14 388	[89]	$LaTiSbO_6$	2 062	876	2 752	14 641	[108]
$BaTiO_3$	1 780	738	2 820	13 862	[90]	$La_4Ti_3O_{12}$ (Ti1)	1 880	518	3 387	14 164	[109]
Ba_2GdNbO_6	**1 931**	**1 278**	**1 904**	**14 513**	[91]	$La_4Ti_3O_{12}$ (Ti2)	1 727	514	3 184	13 498	[109]
Ba_2LaNbO_6	1 780	670	3 290	14 679	[92]	α-$LiAlO_2$	2 345	729	3 139	14 925	[110]
Ba_2CaWO_6	2 139	781	2 924	14 705	[93]	**$LiMgBO_3$**	**2 260**	**1 311**	**3 369**	**15 060**	[111]
$CaAl_2O_4$	2 500	520	3 700	15 198	[94]	**$Li_{1.8}Na_{0.2}TiO_3$**	**2 000**	**1 169**	**2 204**	**14 728**	[112]
$CaAl_{12}O_{19}$	2 132	807	3 088	15 244	[95]	$Li_2Ge_4O_9$	2 222	588	3 253	14 286	[113]
$CaAl_{12}O_{19}$	2 146	750	3 245	15 243	[96]	Li_2TiO_3	1 905	1 058	2 428	14 706	[114]
$CaLi_6La_2Nb_2O_{12}$	2 041	935	2 443	14 065	[97]	$Li_3Mg_2NbO_6$	2 110	828	2 954	14 970	[115]
$CaMg_2Al_{16}O_{27}$	2 137	737	3 247	15 267	[98]	$Li_3Mg_2TaO_6$	2 083	757	3 163	15 129	[116]
$CaYAlO_4$	2 000	879	2 808	14 814	[99]	**$Li_6CaLa_2Sb_2O_{12}$**	**2 045**	**1 250**	**2 174**	**14 285**	[117]
$CaZrO_3$	1 850	754	3 173	15 054	[100]	$MgAl_2O_4$	2 283	800	3 157	15 361	[118]
$CaLaMgNbO_6$	1 984	905	2 603	14 347	[101]	MgO *	1 868	722	3 483	15 809 15 279	[119]
Ca_2LuTaO_6	1 961	933	2 812	15 152	[102]	Mg_2TiO_4	2 089	790	3 172	15 193	[120]
$Ca_3Gd_2W_2O_{12}$	2 105	892	2 530	14 084	[103]	$NaGdCa_4W_2O_{12}$	2 066	847	2 833	14 706	[121]
Ca_3WO_6	2 178	941	2 581	15 036	[93]	$NaLaCa_4W_2O_{12}$	2 083	798	2 745	14 124	[121]
$Ca_{14}Al_{10}Zn_6O_{35}$	2 174	751	2 780	13 947	[104]	**$NaLa_2SbO_6$**	**2 024**	**1243**	**1 866**	**14 144**	[122]
$Ca_{14}Ga_{10}Zn_6O_{35}$	2 140	683	3 020	14 285	[105]	$PbTiO_3$	1 500	780	2 890	14 236	[123]

Tab. 4 (Continue)

Host	*Dq*	*B*	*C*	*E*(^{2}E)	Ref.	Host	*Dq*	*B*	*C*	*E*(^{2}E)	Ref.
$SrAl_3BO_7$	2 128	567	3 573	15 504	[124]					15 361	
$SrMgAl_{10}O_{17}$	2 126	802	3 069	15 151	[125]	$Sr_4Al_{14}O_{25}$ *	2 250	790	3 172	15 384	[131]
$SrTiO_3$	1 821	735	2 812	13 827	[126]					15 457	
Sr_2CaWO_6	2 150	892	2 623	14 925	[93]	$Sr_4Al_{14}O_{25}$	2 222	794	3 232	15 337	[132]
Sr_2GdSbO_6	1 976	826	3 107	15 385	[127]	$Sr_9Gd_2W_4O_{24}$	2 041	697	3 158	14 706	[133]
Sr_2LaSbO_6	2 000	879	2 702	14 814	[128]	TiO_2 anatase	1 830	735	2 816	13 846	[134]
Sr_2YNbO_6	1 952	885	2 912	15 152	[129]	$YAlO_3$	2 100	720	3 025	14 450	[135]
$Sr_4Al_{14}O_{25}$	2 222	680	3 397	15 361	[130]	$Y_2Sn_2O_7$	2 100	700	3 515	15 563	[136]
						$Y_2Ti_2O_7$	2 000	600	3 500	14 956	[136]

* Multicenters and/or various data reported

Tab. 5　Spectroscopic parameters of Mn^{4+} ions in oxyfluoride phosphors, all notations are the same as in Tab. 3

Host	*Dq*	*B*	*C*	*E*(^{2}E)	Ref.	Host	*Dq*	*B*	*C*	*E*(^{2}E)	Ref.
$BaNbOF_5$	2 083	433	4 160	15 948	[137]	K_3MoOF_7	2105	553	3 951	16 155	[144]
$BaTiOF_4$	2 155	577	3 793	15 848	[138]	K_3WOF_7	2 128	609	3 823	16 155	[145]
$CsMoO_2F_3$	2 137	511	3 995	16 000	[139]	$LiAl_4O_6F$	2 185	475	3 791	15 129	[146]
Cs_2NbOF_5	2 110	540	3 937	16 026	[140]	MFG**	2 380	700	3 416	15 576	[147]
$KNaWO_2F_4$	2 088	526	4 004	16 129	[141]	$Na_2WO_2F_4$	2 083	502	4 069	16 155	[148]
$K_2[MoO_2F_4]\cdot H_2O$	2 123	510	4 039	16 129	[142]	Rb_2NbOF_5	2 151	584	3 852	16 077	[149]
$K_3HF_2WO_2F_4$	2 151	836	3 340	16 920	[143]	Sr_2ScO_3F	1 923	736	2 965	14 347	[150]

** 3.5MgO-0.5MgF_2-GeO_2: Mn^{4+}

It can easily be seen that in the fluorides the ^{2}E level is generally located higher than in the oxides. Such an observation has been made earlier[7], and it is attributed to a weaker nephelauxetic effect (weaker covalency) in fluorides. Fig. 1 shows that the emitting ^{2}E level is practically independent of the crystal field strength *Dq*. On the other hand, the energetic separation between the ^{2}E and $^4A_2$ states in the crystal field is very close to the energy interval between the ^{2}G and ^{4}F terms of a free Mn^{4+} ion (these are the terms, where the ^{2}E and $^4A_2$ levels come from-see Fig. 1), which depends on the Racah parameters *B* and *C* only. Since-due to the nephelauxetic effect-the Racah parameters for the impurity ions in solids are reduced (and often quite considerably), when compared to their free ion's values, and the magnitude of such reduction varies to a great extent in different solids due to peculiarities of the chemical bonds formation, the ^{2}E level position depends mainly on the *B* and *C* values. As a consequence, in highly ionic fluorides, the values of the Racah parameters *B* and *C* are generally greater than in more covalent oxides (Tab. 3 and 4), leading to a blue shift of the ^{2}E level. An interesting case is formed by the solids with mixed anion composition, like oxyfluorides (Tab. 5). Since the oxyfluorides combine the fluorides ionicity and the oxide covalency, their emission maxima are positioned between those corresponding to these two large groups of materials.

As a quantitative measure of the covalent effects in the Mn^{4+}-doped crystalline solids, we introduced a non-dimensional parameter β_1, which indicates degree of reduction of the Racah parameters *B* and *C*[28-29,100]:

$$\beta_1 = \sqrt{\left(\frac{B}{B_0}\right)^2 + \left(\frac{C}{C_0}\right)^2}, \qquad (4)$$

where *B*, *C* (B_0, C_0) are the Racah parameters of the corresponding ions in a crystal (free state), respectively. It appears that the position of the ^{2}E energy level is a linear function of this parameter β_1. This linearity follows from the properties of the

Tanabe-Sugano matrices for the d^3 electron configuration, as was derived in Ref. [151]. Fig. 3 illustrates this linear trend. All data points shown in this figure are taken from Tab. 3 – 5 (several entries, which are shown in bold, are omitted, because the reported values of B for those materials exceed the free ion value, thus indicating some problems with the experimental spectra treatment). All data points shown in Fig. 1 were fitted to the linear equation, which was obtained as follows:

$$E(^2\mathrm{E}) = -1140.7 + 16577.1\beta_1, \quad (5)$$

the root-mean-squared deviation σ between the calculated from Eq. (5) and experimental positions of the ^{2}E level was found to be 359 cm^{-1}. Two dashed straight lines in Fig. 3 represent the linear function from Eq. (5) shifted upward and downward by this value of σ. Then nearly all data points are located within this "corridor" marked by the dashed lines. Deviation from the fitting line of Eq. (5) shifted by $\pm\sigma$ can be explained by difficulties in assigning the zero-phonon line (ZPL) of the $^2\mathrm{E}\rightarrow{}^4\mathrm{A}_2$ transition, which is often masked by the vibronic transitions.

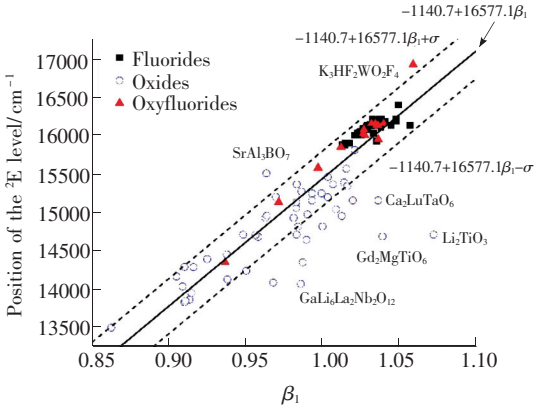

Fig. 3 Dependence of energy of the Mn^{4+} ^{2}E level on the new nephelauxetic ratio β_1

2.3 Tunability of The Mn^{4+} Emission in Crystalline Solids

Analysis of data from Tab. 3 – 5 and Fig. 3 shows that the position of the ^{2}E emitting level varies from 13 498 cm^{-1} (741 nm) in $La_4Ti_3O_{12}$ to 16 920 cm^{-1} (591 nm) in $K_3HF_2WO_2F_4$. In other words, by choosing a proper host, it is possible to tune the Mn^{4+} emission from nearly orange color through deep red to the infrared spectral range, which creates a lot of opportunities for various applications.

The Mn^{4+}-doped phosphors with emission at around 620 nm are very good for the solid-state lighting applications, since such emission is characterized by a greater spectral overlap with the human eye sensitivity curve[152], whereas the deep-red emitting phosphors are more suitable for the agricultural applications as a good light source for effective and fast plant growth[153].

Based on the data presented in this review, it is possible to formulate the following rules that can help in choosing proper hosts for the selected applications:

(1) If red photons in the wavelength range of 600 – 630 nm are needed, then highly ionic fluorides should be considered for doping with the Mn^{4+} ions.

(2) If red photons in the spectral range between 630 nm and 700 nm are required, then highly covalent oxides should be chosen to accommodate the Mn^{4+} ions.

(3) If the local symmetry of the Mn^{4+} site is perfectly octahedral (which means the p-states of ligands and d-states of the Mn^{4+} ions are directed along the same axis), lowering of the ^{2}E level is anticipated due to increased overlap of the above-mentioned wave functions, that leads to a more considerable decrease of the Racah parameters B and C.

(4) If the local symmetry of the Mn^{4+} site is not perfectly octahedral, then the overlap of the p-states of ligands and d-states of the Mn^{4+} ions is decreased, thus leading to the weaker nephelauxetic effect, greater values of the Racah parameters B and C and, as a result, upward shift of the emitting Mn^{4+} ^{2}E level.

(5) External hydrostatic pressure causes decrease of the interionic distances. As a result, this will be accompanied by an increase of the overlap integrals and enhanced nephelauxetic effect. The values of the Racah parameters B and C will be further reduced leading to a slight red shift of the $^2\mathrm{E}\rightarrow{}^4\mathrm{A}_2$ emission transition.

(6) The so-called "chemical" pressure can lead to a similar result. "Chemical" pressure can be produced by partial cation or anion substitution

(especially with greater ionic radii), after which the neighboring chemical bonds will shrink-similar to the hydrostatic pressure. The only difference between these two phenomena is that the "chemical" pressure affects only nearest neighbors around the ion with a greater ionic radius, whereas the hydrostatic pressure acts upon the whole sample.

(7) Fabrication of the Mn-containing nano-sized crystallites gives opportunities to design an exciting class of red luminescence materials showing quantum confinement. The emission color can be tuned by choosing proper size of the crystallites.

2.4 Enhancement of The Mn^{4+} Emission Intensity in Crystalline Solids

An efficient phosphor for the solid-state lighting should produce bright emission after suitable excitation. When it comes to the Mn^{4+} emission spectra, they typically consist of several closely located sharp lines ascribed to the $^2E \rightarrow {}^4A_2$ transition. One of these individual peaks corresponds to the zero-phonon line, the peaks at the higher/lower energy side of it-to the anti-Stokes and Stokes vibronic transitions, respectively. As an empirical rule, intensity of the Stokes peaks is higher than the ZPL and anti-Stokes peaks (relative intensity of these peaks depends on the strength of the electron-vibrational interaction, normal mode energies *etc*). An important question is how to identify the ZPL position. The following example explains this in detail.

Fig. 4 shows the emission spectrum of $NaKSiF_6$: Mn^{4+} [152].

To find the ZPL location, it is necessary to plot the emission spectrum in the energy scale. Then by looking at the spectrum, one has to identify the peak (it may have a very low intensity, sometimes really almost zero), whose position serves as a symmetry point, about which positions of all other peaks in the spectrum become the mirror images of each other. It should be emphasized that the "mirror symmetry" should not be understood literally in this case: the matched peaks intensities are not supposed to match each other, but their positions must differ by approximately the same amount of energy, taken with different signs. The ZPL in Fig. 4 is at about 16 120 cm^{-1} (620 nm). The two nearest peaks located to the left and to the right from it differ by 219 cm^{-1}. This difference corresponds to one of the normal mode energies of the octahedral MnF_6 cluster. The high-energy peak is the anti-Stokes peaks, which is formed by the pure electronic $^2E \rightarrow {}^4A_2$ transition emission transition with absorption of one vibrational quantum (it would increase the energy of the emitted photon), whereas the low-energy peak corresponds to the partial loss of the pure electronic $^2E \rightarrow {}^4A_2$ emission transition energy (one phonon would be produced then). Another pair of emission peaks is mirrored about the ZPL position with the energy difference of about 345 – 348 cm^{-1}. They correspond to the vibronic transitions, which are formed with participation of the pure electronic $^2E \rightarrow {}^4A_2$ transition and another normal mode with the above-given energy.

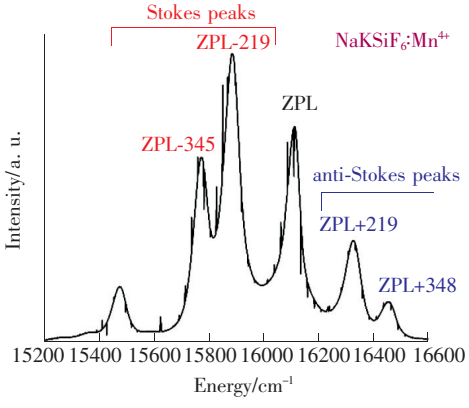

Fig. 4　Emission spectrum of $NaKSiF_6$: Mn^{4+} [152]. The ZPL position and the Stokes/anti-Stokes peaks are indicated.

Fig. 5 shows comparison of the human eye sensitivity

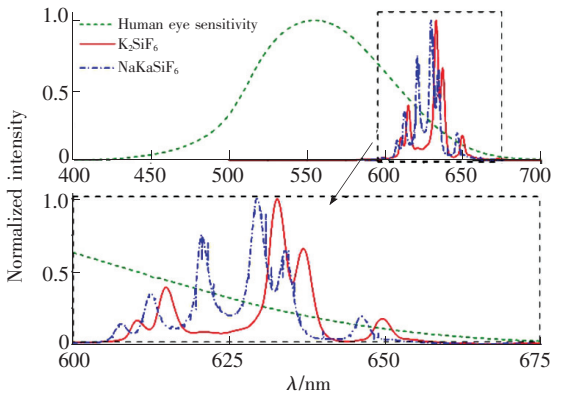

Fig. 5　Human eye sensitivity curve and emission spectra of K_2SiF_6: Mn^{4+} and $NaKSiF_6$: Mn^{4+} phosphors. The figure below is a zoomed view of the area shown by a rectangle in the top figure.

curve peaked at about 550 nm with emission spectra of $K_2SiF_6:Mn^{4+}$ and $NaKSiF_6:Mn^{4+}$ phosphors.

It is clear that the greater the overlap of the emission spectrum with the human eye sensitivity curve is, the brighter the phosphor to the human eye is. From this point of view, the $NaKSiF_6:Mn^{4+}$ phosphor is brighter than $K_2SiF_6:Mn^{4+}$ phosphor, as evidenced by the lower diagram in Fig. 5. Since the Stokes peaks in the emission spectra are more intensive than the ZPL and the anti-Stokes ones (Fig. 4), increase of the ZPL intensity is a very important task to be achieved for getting efficient bright phosphors. In addition, the ZPL for the ideal red phosphors based on the Mn^{4+} ions should be located at about 620 nm-this would ensure a large overlap with the human eye sensitivity curve, still staying in the red part of the visible spectrum.

It has been noticed that the ZPL has a higher intensity in the host materials with rather low local symmetry, especially in those ones, which lack an inversion center at the local site occupied by the emitting impurity ion[152]. This is because the inversion center absence removes the parity selection rule for the electric dipole transitions. Therefore, choosing the low-symmetry hosts for doping with the Mn^{4+} ions is one possible way to get bright phosphors.

It is also possible to remove the inversion center artificially, when making the phosphor, by employing the strategy of the cation or anion substitution. The above given example of $K_2SiF_6:Mn^{4+}$ and $NaKSiF_6:Mn^{4+}$ phosphors is a good illustration. In both phosphors the ZPL is at about 620 nm, but in the latter phosphor its intensity is increased drastically. This is because of random occupation of the first cation site by K and Na the inversion symmetry at the Si site (occupied by the Mn^{4+} ions) is removed. Another example is the Rb_2HfF_6, Cs_2HfF_6, and $RbCsHfF_6$ phosphors with Mn^{4+} ions. By performing the first-principles calculations, it has been shown that in the "mixed" $RbCsHfF_6$ compound the Cs and Rb ions in the second coordination sphere around the Hf ions (occupied by the Mn^{4+} ions after doping) affect the opposite Hf—F chemical bond lengths in the HfF_6 octahedron, which loses then the inversion center[152,154].

We also mention a recent publication[155] that is focused on the ways of achieving higher efficiency and greater stability of the Mn^{4+}-doped phosphors for white LEDs.

2.5 Several Misconceptions Related to The Analysis of The Mn^{4+} Ions Spectra in Crystalline Solids

Quite often it is possible to find examples of improper interpretation and analysis of the Mn^{4+} spectra in solids. Here we shall not give the references to those wrong publications. Instead, we just list those incorrect statements we have seen in the papers and explain what was wrong there.

(1) Sometimes-although not often-the tetrahedral Mn^{4+} centers are mentioned. This is ultimately wrong-the Mn^{4+} ions occupy only octahedral positions.

(2) Sometimes-especially in the oxide hosts-there are certain issues with assignment of the $^4A_2 \rightarrow {}^4T_1$ absorption band. This is because this absorption band overlaps with the O-Mn charge transfer transitions (in fluorides, luckily, this charge transfer band is located at considerably high energy position due to higher electronegativity of the fluoride anion). Then people mistakenly assign the charge transition band to the $^4A_2 \rightarrow {}^4T_1$ transition, which eventually leads to unrealistically high values of the Racah parameter *B*-even exceeding the free ion value (which is physically impossible!) and unrealistically low values of the Racah parameter *C*.

(3) Since the Mn^{4+} ions are always located at the strong crystal field sites ($Dq/B > 2.2 - 2.5$ in the Tanabe-Sugano diagram), the Dq/B ratios which are either smaller or unrealistically higher ($> 5 - 6$, for example) immediately indicate some mistakes in determination of the Dq, B, C values.

(4) There are often some issues with the ZPL determination; *e. g.* people attempt to assign the ZPL to the most intensive peak in the group of vibronic lines corresponding to the $^2E \rightarrow {}^4A_2$ emission transition. This should not be done, and the careful analysis of the ZPL location, as described in the

present review, should be performed.

(5) There are also some attempts to assign the origin of the $^2E \rightarrow {}^4A_2$ emission transition to the electron-vibrational interaction (EVI). This is wrong. The EVI can affect the spectral shape of emission peaks, but the physical origin of appearance of this transition is in the spin-orbit interaction, that mixes together the states with the same total angular momentum $\boldsymbol{J}$ in the ^2G and ^4F terms even for a free ion[17].

(6) The structure of the $^2E \rightarrow {}^4A_2$ emission spectrum is due to the crystal field effects. This is only true partially. The most important reason for the structured $^2E \rightarrow {}^4A_2$ emission spectrum is EVI, and a thorough analysis of the ZPL position and associated vibronics should be performed.

3 Conclusion

In the present review, we have described the main spectroscopic properties of the Mn^{4+} ion, which is a very important activator for the solid-state lighting. The origin of the Mn^{4+} energy levels and their splitting in crystal fields were described. The main advantages of these ions over others are also highlighted. The main spectroscopic parameters of the Mn^{4+} ions in more than 100 solids are collected and the main trend across this group of materials is discussed. Several practical recommendations on how to analyze the spectra of Mn^{4+} ions in crystalline solids are given in detail to help the researchers working in the field for the discovery of novel Mn^{4+} red phosphors.

References:

[1] JÜSTEL T, NIKOL H, RONDA C. New developments in the field of luminescent materials for lighting and displays [J]. *Angew. Chem. Int. Ed.*, 1998, 37(22): 3085-3103.

[2] HÖPPE H A. Recent developments in the field of inorganic phosphors [J]. *Angew. Chem. Int. Ed.*, 2009, 48(20): 3572-3582.

[3] YE S, XIAO F, PAN Y X, *et al.*. Phosphors in phosphor-converted white light-emitting diodes: recent advances in materials, techniques and properties [J]. *Mater. Sci. Eng. R Rep.*, 2010, 71(1): 1-34.

[4] LIN C C, LIU R S. Advances in phosphors for light-emitting diodes [J]. *J. Phys. Chem. Lett.*, 2011, 2(11): 1268-1277.

[5] SMET P F, PARMENTIER A B, POELMAN D. Selecting conversion phosphors for white light-emitting diodes [J]. *J. Electrochem. Soc.*, 2011, 158(6): R37-R54.

[6] XIA Z G, LIU R S. Tunable blue-green color emission and energy transfer of $Ca_2Al_3O_6F$: Ce^{3+}, Tb^{3+} phosphors for near-UV white LEDs [J]. *J. Phys. Chem.* C, 2012, 116(29): 15604-15609.

[7] BRIK M G, SRIVASTAVA A M. On the optical properties of the Mn^{4+} ion in solids [J]. *J. Lumin.*, 2013, 133: 69-72.

[8] SHANG M M, LI C X, LIN J. How to produce white light in a single-phase host? [J]. *Chem. Soc. Rev.*, 2014, 43(5) 1372-1386.

[9] BÜNZLI J C G. On the design of highly luminescent lanthanide complexes [J]. *Chem. Soc. Rev.*, 2015, 293-294: 19-47.

[10] LI J H, YAN J, WEN D W, *et al.*. Advanced red phosphors for white light-emitting diodes [J]. *J. Mater. Chem.* C, 2016, 4(37): 8611-8623.

[11] LIN C C, MEIJERINK A, LIU R S. Critical red components for next-generation white LEDs [J]. *J. Phys. Chem. Lett.*, 2016, 7(3): 495-503.

[12] XIA Z G, MEIJERINK A. Ce^{3+}-doped garnet phosphors: composition modification, luminescence properties and applications [J]. *Chem. Soc. Rev.*, 2017, 46(1): 275-299.

[13] LIU R S. *Phosphors, Up Conversion Nano Particles, Quantum Dots and Their Applications* [M]. Berlin, Heidelberg: Springer, 2017.

[14] ZHOU Q, DOLGOV L, SRIVASTAVA A M, *et al.*. Mn^{2+} and Mn^{4+} red phosphors: synthesis, luminescence and applications in WLEDs. A review [J]. *J. Mater. Chem.* C, 2018, 6(11): 2652-2671.

[15] BRIK M G, MA C G. *Theoretical Spectroscopy of Transition Metal and Rare Earth Ions: From Free State to Crystal Field*

[M]. Singapore:Jenny Stanford Publishing, 2020.

[16] AVRAM N M,BRIK M G. *Optical Properties of 3d-ions in Crystals:Spectroscopy and Crystal Field Analysis* [M]. Beijing: Tsinghua University Press, 2013.

[17] BRIK M G,SRIVASTAVA A M. Critical review—a review of the electronic structure and optical properties of ions with d^3 electron configuration (V^{2+},Cr^{3+},Mn^{4+},Fe^{5+}) and main related misconceptions [J]. *ECS J. Sol. State Sci. Technol.*, 2018,7(1):R3079-R3085.

[18] MORRISON C A. *Crystal Fields for Transition-Metal Ions in Laser Host Materials* [M]. Berlin,Heidelberg:Springer-Verlag, 1992.

[19] HENDERSON B,IMBUSCH G F. *Optical Spectroscopy of Inorganic Solids* [M]. Oxford:Clarendon Press, 1989.

[20] NAKAMURA S, MUKAI T, SENOH M. Candela-class high-brightness InGaN/AlGaN double-heterostructure blue-light-emitting diodes [J]. *Appl. Phys. Lett.*, 1994,64(13):1687-1689.

[21] NAKAMURA S,SENOH M,NAGAHAMA S,*et al.*. InGaN-based multi-quantum-well-structure laser diodes [J]. *Jpn. J. Appl. Phys.*, 1996,35(1B):L74-L76.

[22] SETLUR A A,RADKOV E V,HENDERSON C S,*et al.*. Energy-efficient,high-color-rendering LED lamps using oxyfluoride and fluoride phosphors [J]. *Chem. Mater.*, 2010,22(13):4076-4082.

[23] SIJBOM H F,VERSTRAETE R,JOOS J J,*et al.*. $K_2SiF_6:Mn^{4+}$ as a red phosphor for displays and warm-white LEDs:a review of properties and perspectives [J]. *Opt. Mater. Exp.*, 2017,7(9):3332-3365.

[24] BEERS W W,SMITH D,COHEN W E,*et al.*. Temperature dependence(13 – 600 K) of Mn^{4+} lifetime in commercial $Mg_{28}Ge_{7.55}O_{32}F_{15.04}$ and K_2SiF_6 phosphors [J]. *Opt. Mater.*, 2018,84:614-617.

[25] RADKOV E V,GRIGOROV L S,SETLUR A A,*et al.*. Red line emitting phosphor materials for use in LED applications: US,7497973 [P]. 2009-03-03.

[26] RADKOV E V,SETLUR A A,SRIVASTAVA A M,*et al.*. Red line emitting phosphors for use in led applications:US, 7648649 [P]. 2010-01-19.

[27] GARCIA-SANTAMARIA F,MURPHY J E,SETLUR A A,*et al.*. Concentration quenching in $K_2SiF_6:Mn^{4+}$ phosphors [J]. *ECS J. Solid State Sci. Technol.*, 2018,7(1):R3030-R3033.

[28] BRIK M G,CAMARDELLO S J,SRIVASTAVA A M. Influence of covalency on the $Mn^{4+}\ ^2E_g \rightarrow {}^4A_{2g}$ emission energy in crystals [J]. *ECS J. Solid State Sci. Technol.*, 2015,4(3):R39-R43.

[29] BRIK M G,CAMARDELLO S J,SRIVASTAVA A M,*et al.*. Spin-forbidden transitions in the spectra of transition metal ions and nephelauxetic effect [J]. *ECS J. Solid State Sci. Technol.*, 2016,5(1):R3067-R3077.

[30] ADACHI S. Review-Tanabe-Sugano energy-level diagram and racah parameters in Mn^{4+}-activated red and deep red-emitting phosphors [J]. *ECS J. Solid State Sci. Technol.*, 2019,8(12):R183-R196.

[31] SEKIGUCHI D,ADACHI S. Synthesis and photoluminescence spectroscopy of $BaGeF_6:Mn^{4+}$ red phosphor [J]. *Opt. Mater.*, 2015,42:417-422.

[32] SEKIGUCHI D,NARA J,ADACHI S. Photoluminescence and raman scattering spectroscopies of $BaSiF_6:Mn^{4+}$ red phosphor [J]. *J. Appl. Phys.*, 2013,113(18):183516-1-6.

[33] XI L Q,PAN Y X. Tailored photoluminescence properties of a red phosphor $BaSnF_6:Mn^{4+}$ synthesized from Sn metal at room temperature and its formation mechanism [J]. *Mater. Res. Bull.*, 2017,86:57-62.

[34] SEKIGUCHI D,ADACHI S. Synthesis and optical properties of $BaTiF_6:Mn^{4+}$ red phosphor [J]. *ECS J. Solid State Sci. Technol.*, 2014,3(4):R60-R64.

[35] DENG T T,SONG E H,ZHOU Y Y,*et al.*. Tailoring photoluminescence stability in double perovskite red phosphors $A_2BAlF_6:Mn^{4+}$ (A = Rb, Cs; B = K, Rb) *via* neighboring-cation modulation [J]. *J. Mater. Chem.* C, 2017,5(47): 12422-12429.

[36] BARANDIARÁN Z,SEIJO L. Alternative configuration interaction expansions for transition metal ions with intermediate oxidation states in crystals:the structure and absorption spectrum of $Cs_2GeF_6:Mn^{4+}$ [J]. *J. Chem. Phys.*, 2001,115(15): 7061-7065.

[37] SENDEN T,VAN HARTEN E J,MEIJERINK A. Synthesis and narrow red luminescence of $Cs_2HfF_6:Mn^{4+}$,a new phosphor for warm white LEDs [J]. *J. Lumin.*, 2018,194:131-138.

[38] ZHANG J F,LIU L L,HE S G,*et al.*. Cs_2MnF_6 red phosphor with ultrahigh absorption efficiency [J]. *Inorg. Chem.*,

2019,58(22):15207-15215.

[39] ZHOU Y Y,SONG E H,BRIK M G,*et al.*. Non-equivalent Mn^{4+} doping into A_2NaScF_6 (A = K,Rb,Cs) hosts toward short fluorescence lifetime for backlight display application [J]. *J. Mater. Chem.* C, 2019,7(30):9203-9210.

[40] XU Y K,ADACHI S. Properties of Mn^{4+}-activated hexafluorotitanate phosphors [J]. *J. Electrochem. Soc.*, 2011,158(3):J58-J65.

[41] ARAI Y,ADACHI S. Optical properties of Mn^{4+}-activated Na_2SnF_6 and Cs_2SnF_6 red phosphors [J]. *J. Lumin.*, 2011,131(12):2652-2660.

[42] ZHOU Q,TAN H Y,ZHOY Y Y,*et al.*. Optical performance of Mn^{4+} in a new hexa-coordinated fluorozirconate complex of Cs_2ZrF_6[J]. *J. Mater. Chem.* C, 2016,4(31):7443-7448.

[43] MING H,ZHANG J F,LIU L L,*et al.*. Luminescent properties of a Cs_3AlF_6: Mn^{4+} red phosphor for warm white light-emitting diodes [J]. *ECS J. Sol. State Sci. Technol.*, 2018,7(9):R149-R155.

[44] KUMADA N,YANAGIDA S,TAKEI T,*et al.*. Hydrothermal synthesis and crystal structure of new red phosphors, KNa$M$$F_7$: Mn^{4+} (M:Nb,Ta) [J]. *Mater. Res. Bull.*, 2019,115:170-175.

[45] DENG T T,SONG E H,SU J,*et al.*. Stable narrowband red emission in fluorotellurate $KTeF_5$: Mn^{4+} *via* Mn^{4+} noncentral-site occupation [J]. *J. Mater. Chem.* C, 2018,6(16):4418-4426.

[46] HU T,LIN H,LIN F L,*et al.*. Narrow- band red- emitting $KZnF_3$: Mn^{4+} fluoroperovskites:insights into electronic/vibronic transition and thermal quenching behavior [J]. *J. Mater. Chem.* C, 2018,6(40) 10845-10854.

[47] ADACHI S,TAKAHASHI T. Photoluminescent properties of K_2GeF_6: Mn^{4+} red phosphor synthesized from aqueous HF/$KMnO_4$ solution [J]. *J. Appl. Phys.*, 2009,106(1):013516-1-6.

[48] TAKAHASHI T, ADACHI S. Mn^{4+}-activated red photoluminescence in K_2SiF_6 phosphor [J]. *J. Electrochem. Soc.*, 2008,155(12):E183-E188.

[49] ZHU Y W,YUAN S,LIN H,*et al.*. Optimizing and adjusting the photoluminescence of Mn^{4+}-doped fluoride phosphors via forming composite particles [J]. *Dalton Trans.*, 2019,48(2):711-717.

[50] ZHU Y W,YU J B,LIU Y,*et al.*. Photoluminescence properties of a novel red fluoride K_2LiGaF_6: Mn^{4+} nanophosphor [J]. *RSC Adv.*, 2017,7(49):30588-30593.

[51] KASA R,ARAI Y,TAKAHASHI T,*et al.*. Photoluminescent properties of cubic K_2MnF_6 particles synthesized in metal immersed HF/$KMnO_4$ solutions [J]. *J. Appl. Phys.*, 2010,108(11):113503-1-6.

[52] ZHU Y W,CAO L Y,BRIK M G,*et al.*. Facile synthesis,morphology and photoluminescence of a novel red fluoride nanophosphor K_2NaAlF_6: Mn^{4+} [J]. *J. Mater. Chem.* C, 2017,5(26):6420-6426.

[53] JIANG C Y,BRIK M G,LI L H,*et al.*. The electronic and optical properties of a narrow-band red-emitting nanophosphor K_2NaGaF_6: Mn^{4+} for warm white light-emitting diodes [J]. *J. Mater. Chem.* C, 2018,6(12):3016-3025.

[54] MING H,LIU L L,HE S G,*et al.*. An ultra-high yield of spherical K_2NaScF_6: Mn^{4+} red phosphor and its application in ultra-wide color gamut liquid crystal displays [J]. *J. Mater. Chem.* C, 2019,7(24):7237-7248.

[55] MING H,ZHANG J F,LIU S F,*et al.*. A green synthetic route to K_2NbF_7: Mn^{4+} red phosphor for the application in warm white LED devices [J]. *Opt. Mater.*, 2018,86:352-359.

[56] WEI L L,LIN C C,FANG M H,*et al.*. A low-temperature co-precipitation approach to synthesize fluoride phosphors K_2MF_6: Mn^{4+} (M = Ge,Si) for white LED applications [J]. *J. Mater. Chem.* C, 2015,3(8):1655-1660.

[57] KASA R,ADACHI S. Red and deep red emissions from cubic K_2SiF_6: Mn^{4+} and hexagonal K_2MnF_6 synthesized in HF/$KMnO_4$/KHF_2/Si solutions [J]. *J. Electrochem. Soc.*, 2012,159(4):J89-J95.

[58] LIN H,HU T,HUANG Q M,*et al.*. Non-rare-earth K_2XF_7: Mn^{4+} (X = Ta,Nb):a highly- efficient narrow-band red phosphor enabling the application in wide-color-gamut LCD [J]. *Laser Photon. Rev.*, 2017,11(6):1700148.

[59] HUANG D C,ZHU H M,DENG Z H,*et al.*. Moisture-resistant Mn^{4+}-doped core-shell-structured fluoride red phosphor exhibiting high luminous efficacy for warm white light-emitting diodes [J]. *Angew. Chem. Int. Ed.*, 2019,58(12):3843-3847.

[60] WANG T M,GAO Y,CHEN Z P,*et al.*. The formation of KF induced red-emitting phosphors K_2TiF_6 · $BaF(HF_2)$: Mn^{4+} by cation exchange [J]. *J. Lumin.*, 2017,188:307-312.

[61] DENG T T,SONG E H,ZHOU Y Y,*et al.*. Stable narrowband red phosphor K_3GaF_6: Mn^{4+} derived from hydrous K_2GaF_5(H_2O) and K_2MnF_6[J]. *J. Mater. Chem.* C, 2017,5(37):9588-9596.

[62] MING H, LIU S F, LIU L L, *et al.*. Highly regular, uniform K_3ScF_6: Mn^{4+} phosphors: facile synthesis, microstructures, photoluminescence properties, and application in light-emitting diode devices [J]. *ACS Appl. Mater. Interfaces*, 2018, 10(23): 19783-19795.

[63] TAN H Y, RONG M Z, ZHOU Y Y, *et al.*. Luminescence behaviour of Mn^{4+} ions in seven coordination environments of K_3ZrF_7 [J]. *Dalton Trans.*, 2016, 45(23): 9654-9660.

[64] ZHU M M, PAN Y X, WU M M, *et al.*. Optimized photoluminescence properties of a novel red phosphor $LiSrAlF_6$: Mn^{4+} synthesized at room-temperature [J]. *J. Alloys Compd.*, 2019, 774: 331-337.

[65] ZHU M M, PAN Y X, WU M M, *et al.*. Synthesis and improved photoluminescence of a novel red phosphor $LiSrGaF_6$: Mn^{4+} for applications in warm WLEDs [J]. *Dalton Trans.*, 2018, 47(37): 12944-12950.

[66] ZHU M M, PAN Y X, CHEN X, *et al.*. Formation mechanism and optimized luminescence of Mn^{4+}-doped unequal dual-alkaline hexafluorosilicate $Li_{0.5}Na_{1.5}SiF_6$ [J]. *J. Am. Ceram. Soc.*, 2018, 101(11): 4983-4993.

[67] ZHU M M, PAN Y X, XI L Q, *et al.*. Design, preparation, and optimized luminescence of a dodec-fluoride phosphor $Li_3Na_3Al_2F_{12}$: Mn^{4+} for warm WLED applications [J]. *J. Mater. Chem.* C, 2017, 5(39): 10241-10250.

[68] ZHU M M, PAN Y X, HUANG Y Q, *et al.*. Designed synthesis, morphology evolution and enhanced photoluminescence of a highly efficient red dodec-fluoride phosphor, $Li_3Na_3Ga_2F_{12}$: Mn^{4+}, for warm WLEDs [J]. *J. Mater. Chem.* C, 2018, 6(3): 491-499.

[69] HONG F, CHENG H M, SONG C, *et al.*. Novel polygonal structure Mn^{4+} activated In^{3+}-based Elpasolite-type hexafluorides red phosphor for warm white light-emitting diodes (WLEDs) [J]. *Dalton Trans.*, 2019, 48(4): 1376-1385.

[70] WANG Y J, Zhou Y Y, SONG E H. Ammonium salt conversion towards Mn^{4+} doped $(NH_4)_2NaScF_6$ narrow-band red-emitting phosphor [J]. *J. Alloys Compd.*, 2019, 811: 151945.

[71] BIN HUMAYOUN U, KWON S B, SAMI S K, *et al.*. $(NH_4)_3AlF_6$: Mn^{4+} a novel red phosphor—facile synthesis, structure and luminescence characteristics [J]. *J. Alloys Compd.*, 2019, 776: 594-598.

[72] SETLUR A A, MURPHY J E, SISTA S P. Quenching in Mn^{4+}-complex fluoride phosphors: initial relationships based upon $NaKSiF_6$: Mn^{4+} [J]. *ECS J. Solid State Sci. Technol.*, 2020, 9(1): 016018-1-4.

[73] FANG M H, WU W L, JIN Y, *et al.*. Control of luminescence by tuning of crystal symmetry and local structure in Mn^{4+}-activated narrow band fluoride phosphors [J]. *Angew. Chem. Int. Ed.*, 2018, 57(7): 1797-1801.

[74] XU Y K, ADACHI S. Properties of Na_2SiF_6: Mn^{4+} and Na_2GeF_6: Mn^{4+} red phosphors synthesized by wet chemical etching [J]. *J. Appl. Phys.*, 2009, 105(1): 013525-1-6.

[75] LIU Y M, LI Y L, HUANG W J, *et al.*. Enhancement of zero phonon line for Na_2TiF_6: Mn^{4+}, Li^+ phosphors induced by Li^+ [J]. *J. Mater. Sci.: Mater. Electron.*, 2019, 30(15): 14646-14656.

[76] SONG E H, WANG J Q, YE S, *et al.*. Room-temperature synthesis and warm-white LED applications of Mn^{4+} ion doped fluoroaluminate red phosphor Na_3AlF_6: Mn^{4+} [J]. *J. Mater. Chem.* C, 2016, 4(13): 2480-2487.

[77] XU H P, HONG F, PANG G, *et al.*. Co-precipitation synthesis, luminescent properties and application in warm WLEDs of Na_3GaF_6: Mn^{4+} red phosphor [J]. *J. Lumin.*, 2020, 219: 116960.

[78] FANG M H, YANG T H, LESNIEWSKI T, *et al.*. Hydrogen-containing $Na_3HTi_{1-x}Mn_xF_8$ narrow-band phosphor for light-emitting diodes [J]. *ACS Energy Lett.*, 2019, 4(2): 527-533.

[79] KIM M, PARK W B, LEE J W, *et al.*. Rb_3SiF_7: Mn^{4+} and Rb_2CsSiF_7: Mn^{4+} red-emitting phosphors with a faster decay rate [J]. *Chem. Mater.*, 2018, 30(19): 6936-6944.

[80] WU W L, FANG M H, ZHOU W L, *et al.*. High color rendering index of Rb_2GeF_6: Mn^{4+} for light-emitting diodes [J]. *Chem. Mater.*, 2017, 29(3): 935-939.

[81] WANG L Y, SONG E H, ZHOU Y Y, *et al.*. An efficient and stable narrow band Mn^{4+}- activated fluorotitanate red phosphor Rb_2TiF_6: Mn^{4+} for warm white LED applications [J]. *J. Mater. Chem.* C, 2018, 6(32): 8670-8678.

[82] JIANG C Y, BRIK M G, SRIVASTAVA A M, *et al.*. Significantly conquering moisture-induced luminescence quenching of red line-emitting phosphor Rb_2SnF_6: Mn^{4+} through $H_2C_2O_4$ triggered particle surface reduction for blue converted warm white light-emitting diodes [J]. *J. Mater. Chem.* C, 2019, 7(2) 247-255.

[83] DENG T T, SONG E H, ZHOU Y Y, *et al.*. Implementation of high color quality, high luminous warm WLED using efficient and thermally stable Rb_3AlF_6: Mn^{4+} as red color converter [J]. *J. Alloys Compd.*, 2019, 795: 453-461.

[84] JANG S, PARK J K, KIM M, *et al.*. New red-emitting phosphor $Rb_xK_{3-x}SiF_7$: Mn^{4+} ($x=0,1,2,3$): DFT predictions and

synthesis [J]. *RSC Adv.*, 2019, 9: 39589-39594.

[85] LV L F, JIANG X N, PAN Y X, *et al.*. Luminescence properties and thermal stability of a red phosphor $ZnSiF_6 \cdot 6H_2O$: Mn^{4+} synthesized by the one-step hydrothermal method [J]. *J. Lumin.*, 2014, 152: 214-217.

[86] HOSHINO R, ADACHI S. Optical spectroscopy of $ZnSiF_6 \cdot 6H_2O$: Mn^{4+} red phosphor [J]. *J. Appl. Phys.*, 2013, 114(21): 213502-1-6.

[87] ZHONG J S, CHEN D Q, WANG X, *et al.*. Synthesis and optical performance of a new red-emitting $ZnTiF_6 \cdot 6H_2O$: Mn^{4+} phosphor for warm white-light-emitting diodes [J]. *J. Alloys Compd.*, 2016, 662: 232-239.

[88] ZHENG W C. Investigations of the zero-field splitting and the first excited state splitting and their stress dependences for Al_2O_3: Mn^{4+} [J]. *J. Phys. Chem. Solids*, 1999, 60(3): 359-361.

[89] LAN Y W, SUN Z H, LU Z Z, *et al.*. Synthesis, luminescence property, and application of a novel red-emitting $BaLaZnTaO_6$: Mn^{4+} phosphor [J]. *Opt. Laser Technol.*, 2019, 119: 105614.

[90] WU X X, FANG W, FENG W L, *et al.*. Electron paramagnetic resonance parameters of Mn^{4+} ion in h-$BaTiO_3$ crystal from a two-mechanism model [J]. *Pramana*, 2009, 72(3): 569-575.

[91] HUANG D Y, DANG P P, LIAN H Z, *et al.*. Luminescence and energy-transfer properties in Bi^{3+}/Mn^{4+}-codoped Ba_2GdNbO_6 double-perovskite phosphors for white-light-emitting diodes [J]. *Inorg. Chem.*, 2019, 58(22): 15507-15519.

[92] SRIVASTAVA A M, BRIK M G. *Ab initio* and crystal field studies of the Mn^{4+}- doped Ba_2LaNbO_6 double-perovskite [J]. *J. Lumin.*, 2012, 132(3): 579-584.

[93] QIN L, WEI D L, BI S, *et al.*. Comparative study of Mn^{4+} $2E_g \rightarrow {}^4A_{2g}$ luminescence in isostructural A_2CaWO_6 (A = Ca, Sr, Ba) with double perovskite structure [J]. *Opt. Mater.*, 2019, 98: 109496.

[94] CAO R P, ZHANG F X, CAO C Y, *et al.*. Synthesis and luminescence properties of $CaAl_2O_4$: Mn^{4+} phosphor [J]. *Opt. Mater.*, 2014, 38: 53-56.

[95] MURATA T, TANOUE T, IWASAKI M, *et al.*. Fluorescence properties of Mn^{4+} in $CaAl_{12}O_{19}$ compounds as red-emitting phosphor for white LED [J]. *J. Lumin.*, 2005, 114(3-4): 207-212.

[96] BRIK M G, PAN Y X, LIU G K. Spectroscopic and crystal field analysis of absorption and photoluminescence properties of red phosphor $CaAl_{12}O_{19}$: Mn^{4+} modified by MgO [J]. *J. Alloys Compd.*, 2011, 509(5): 1452-1456.

[97] HUANG D Y, DANG P P, WEI Y, *et al.*. A deep-red-emitting Bi^{3+}/Mn^{4+}-doped $CaLi_6La_2Nb_2O_{12}$ phosphor: luminescence and energy transfer properties [J]. *Mater. Res. Bull.*, 2020, 124: 110743.

[98] WANG B, LIN H, XU J, *et al.*. $CaMg_2Al_{16}O_{27}$: Mn^{4+}-based red phosphor: a potential color converter for high-powered warm W-LED [J]. *ACS Appl. Mater. Interfaces*, 2014, 6(24): 22905-22913.

[99] ZHANG Y L, HUANG Y D, LI M H, *et al.*. Tuning the luminescence properties of Mn^{4+}-activated $CaYAlO_4$ phosphor by co-doping cations for indoor plant cultivation [J]. *J. Am. Ceram. Soc.*, 2020, 103(8): 4373-4383.

[100] BRIK M G, SRIVASTAVA A M. Electronic energy levels of the Mn^{4+} ion in the perovskite, $CaZrO_3$ [J]. *ECS J. Solid State Sci. Technol.*, 2013, 2(7): R148-R152.

[101] SHI L, HAN Y J, WANG S, *et al.*. Synthesis and luminescence properties of $CaLaMgNbO_6$: Mn^{4+} red phosphor for UV-based w-LEDs [J]. *Mod. Phys. Lett.* B, 2019, 33(34): 1950426.

[102] HUANG X Y, SUN Q, DEVAKUMAR B. Novel efficient deep-red-emitting Ca_2LuTaO_6: Mn^{4+} double-perovskite phosphors for plant growth LEDs [J]. *J. Lumin.*, 2020, 222: 117177.

[103] SHI L, HAN Y J, JI Z X, *et al.*. Photoluminescence properties of novel far-red emission $Ca_3Gd_2W_2O_{12}$: Mn^{4+} phosphor [J]. *Russ. J. Phys. Chem.* A, 2019, 93(11): 2306-2313.

[104] DING Y, GUO N, Lü X, *et al.*. None-rare-earth activated $Ca_{14}Al_{10}Zn_6O_{35}$: Bi^{3+}, Mn^{4+} phosphor involving dual luminescent centers for temperature sensing [J]. *J. Am. Ceram. Soc.*, 2019, 102(12): 7436-7447.

[105] ZHONG Y, GAI S J, XIA M, *et al.*. Enhancing quantum efficiency and tuning photoluminescence properties in far-red-emitting phosphor $Ca_{14}Ga_{10}Zn_6O_{35}$: Mn^{4+} based on chemical unit engineering [J]. *Chem. Eng. J.*, 2019, 374: 381-391.

[106] SRIVASTAVA A M, BEERS W W. Luminescence of Mn^{4+} in the distorted perovskite Gd_2MgTiO_6 [J]. *J. Electrochem. Soc.*, 1996, 143(9): L203-L205.

[107] SRIVASTAVA A M, BRIK M G. Crystal field studies of the Mn^{4+} energy levels in the perovskite, $LaAlO_3$ [J]. *Opt. Mater.*, 2013, 35(8): 1544-1548.

[108] LUO H Y, LI X G, WANG X, *et al.*. Highly thermal-sensitive robust $LaTiSbO_6$: Mn^{4+} with a single-band emission and its topological architecture for single/dual-mode optical thermometry [J]. *Chem. Eng. J.*, 2020, 384: 123272.

[109] JI H P, UEDA J, BRIK M G, *et al.*. Intense deep-red zero phonon line emission of Mn^{4+} in double perovskite $La_4Ti_3O_{12}$ [J]. *Phys. Chem. Chem. Phys.*, 2019, 21(45): 25108-25117.

[110] AOYAMA M, AMANO Y, INOUE K, *et al.*. Synthesis and characterization of Mn-activated lithium aluminate red phosphors [J]. *J. Lumin.*, 2013, 136: 411-414.

[111] BEDYAL A K, KUNTI A K, MENON S G, *et al.*. Red emitting non-rare earth doped $LiMgBO_3$ phosphor for light emitting diodes [J]. *J. Alloys Compd.*, 2020, 830: 154622.

[112] SEKULIĆ M, RISTIĆ Z, MILIĆ EVIĆ B, *et al.*. $Li_{1.8}Na_{0.2}TiO_3$: Mn^{4+}: the highly sensitive probe for the low-temperature lifetime-based luminescence thermometry [J]. *Opt. Commun.*, 2019, 452: 342-346.

[113] CAO Y R, FANG Y Z, ZHANG G H, *et al.*. High quantum yield red-emission phosphor $Li_2Ge_4O_9$: Mn^{4+} for WLEDs application [J]. *Opt. Mater.*, 2019, 98: 109442.

[114] HASEGAWA T, NISHIWAKI Y, FUJISHIRO F, *et al.*. Quantitative determination of the effective Mn^{4+} concentration in a Li_2TiO_3: Mn^{4+} phosphor and its effect on the photoluminescence efficiency of deep red emission [J]. *ACS Omega*, 2019, 4(22): 19856-19862.

[115] WANG X C, ZHOU X P, CAO Y X, *et al.*. Insight into a novel rare-earth-free red-emitting phosphor $Li_3Mg_2NbO_6$: Mn^{4+}: structure and luminescence properties [J]. *J. Am. Ceram. Soc.*, 2019, 102(11): 6724-6731.

[116] WANG S Y, SUN Q, LIANG J, *et al.*. Preparation and photoluminescence properties of novel Mn^{4+} doped $Li_3Mg_2TaO_6$ red-emitting phosphors [J]. *Inorg. Chem. Commun.*, 2020, 116: 107903.

[117] HAN Y J, WANG S, LIU H, *et al.*. A novel Al^{3+} modified $Li_6CaLa_2Sb_2O_{12}$: Mn^{4+} far -red-emitting phosphor with garnet structure for plant cultivation [J]. *J. Lumin.*, 2020, 221: 117031.

[118] JI H P, HOU X H, MOLOKEEV M S, *et al.*. Ultrabroadband red luminescence of Mn^{4+} in $MgAl_2O_4$ peaking at 651 nm [J]. *Dalton Trans.*, 2020, 49(17): 5711-5721.

[119] WU X X, FANG W, FENG W L, *et al.*. Study of EPR parameters and defect structure for two tetragonal impurity centers in MgO: Cr^{3+} and MgO: Mn^{4+} crystals [J]. *Appl. Magn. Reson.*, 2009, 35(4): 503-510.

[120] MEDIĆ M M, BRIK M G, DRAŽIĆ G, *et al.*. Deep-red emitting Mn^{4+} doped Mg_2TiO_4 nanoparticles [J]. *J. Phys. Chem. C*, 2015, 119(1): 724-730.

[121] LI K, VAN DEUN R. Insight into emission-tuning and luminescence thermal quenching investigations in $NaLa_{1-x}Gd_xCa_4W_2O_{12}$: Mn^{4+} phosphors *via* the ionic couple substitution of $Na^+ + Ln^{3+}$ (Ln = La, Gd) for $2Ca^{2+}$ in $Ca_6W_2O_{12}$: Mn^{4+} for plant-cultivation LED applications [J]. *Dalton Trans.*, 2019, 48(42): 15936-15941.

[122] SHI L, HAN Y J, WANG S, *et al.*. $NaLa_2SbO_6$: Mn^{4+} far-red phosphor: synthesis, luminescence properties and emission enhancement by Al^{3+} ions [J]. *J. Lumin.*, 2020, 219: 116865.

[123] WU X X, ZHENG W C, FANG W. Theoretical investigations of the EPR parameters for Cr^{3+} and Mn^{4+} ions in $PbTiO_3$ crystals [J]. *Spectrochim. Acta A*, 2008, 69(2): 498-502.

[124] ZHONG Y, ZHOU N, XIA M, *et al.*. Synthesis and photoluminescence properties of novel red-emitting phosphor $SrAl_3BO_7$: Mn^{4+} with enhanced emission by $Mg^{2+}/Zn^{2+}/Ca^{2+}$ incorporation for plant growth LED lighting [J]. *Ceram. Int.*, 2019, 45(17): 23528-23539.

[125] MENG L L, LIANG L F, WEN Y X. Deep red phosphors $SrMgAl_{10}O_{17}$: Mn^{4+}, M (M = Li^+, Na^+, K^+, Cl^-) for warm white light emitting diodes [J]. *J. Mater. Sci.: Mater. Electron.*, 2014, 25(6): 2676-2681.

[126] BRYKNAR Z. Application of spectroscopic probes in study of ferroelectrics [J]. *Ferroelectrics*, 2004, 298(1): 43-48.

[127] SHI L, WANG S, HAN Y J, *et al.*. Effects of Ti^{4+}- and W^{6+}-substitution on photoluminescence properties of Sr_2GdSbO_6: Mn^{4+} phosphor for plant cultivation [J]. *J. Alloys Compd.*, 2020: 829: 154475.

[128] SHI L, WANG S, HAN Y J, *et al.*. Sr_2LaSbO_6: Mn^{4+} far-red phosphor for plant cultivation: synthesis, luminescence properties and emission enhancement by Al^{3+} ions [J]. *J. Lumin.*, 2020, 221: 117091.

[129] SHI L, HAN Y J, JI Z X, *et al.*. Effects of Al^{3+}-substitution on photoluminescence properties of Sr_2YNbO_6: Mn^{4+} far-red phosphor for plant cultivation [J]. *J. Lumin.*, 2020, 218: 116828.

[130] XU Y D, WANG D, WANG L, *et al.*. Preparation and luminescent properties of a new red phosphor ($Sr_4Al_{14}O_{25}$: Mn^{4+}) for white LEDs [J]. *J. Alloys Compd.*, 2013, 550: 226-230.

[131] PENG M Y, YIN X W, TANNER P A, *et al.*. Site occupancy preference, enhancement mechanism, and thermal resistance of Mn^{4+} red luminescence in $Sr_4Al_{14}O_{25}:Mn^{4+}$ for warm WLEDs [J]. *Chem. Mater.*, 2015, 27(8): 2938-2945.

[132] CHEN L, DENG X R, ZHAO E L, *et al.*. The effect of electron cloud expansion on the red luminescence of $Sr_4Al_{14}O_{25}:Mn^{4+}$ revealed by calculation of the Racah parameters [J]. *J. Alloys Compd.*, 2014, 613: 312-316.

[133] HAN Y J, WANG S, LIU H, *et al.*. Mn^{4+}-doped tetratungstate $Sr_9Gd_2W_4O_{24}$ far-red phosphor: synthesis, luminescence properties, and potential applications in indoor plant cultivation [J]. *J. Lumin.*, 2020, 220: 117027.

[134] WU X X, FENG W L, ZHENG W C. Investigations of EPR parameters for Cr^{3+} and Mn^{4+} ions in anatase (TiO_2) crystals [J]. *Phys. Stat. Sol.* (b), 2007, 244(9): 3347-3351.

[135] BRIK M G, SILDOS I, BERKOWSKI M, *et al.*. Spectroscopic and crystal field studies of $YAlO_3$ single crystals doped with Mn ions [J]. *J. Phys.: Condens. Matter*, 2009, 21(2): 025404-1-5.

[136] BRIK M G, SRIVASTAVA A M, AVRAM N M. Comparative analysis of crystal field effects and optical spectroscopy of six-coordinated Mn^{4+} ion in the $Y_2Ti_2O_7$ and $Y_2Sn_2O_7$ pyrochlores [J]. *Opt. Mater.*, 2011, 33(11): 1671-1676.

[137] DONG X L, PAN Y X, LI D, *et al.*. A novel red phosphor of Mn^{4+} ion-doped oxyfluoroniobate $BaNbOF_5$ for warm WLED applications [J]. *CrystEngComm*, 2018, 20(37): 5641-5646.

[138] LIANG Z B, YANG Z F, TANG H J, *et al.*. Synthesis, luminescence properties of a novel oxyfluoride red phosphor $BaTiOF_4:Mn^{4+}$ for LED backlighting [J]. *Opt. Mater.*, 2019, 90: 89-94.

[139] HE S G, XU F F, HAN T T, *et al.*. A Mn^{4+}-doped oxyfluoride phosphor with remarkable negative thermal quenching and high color stability for warm WLEDs [J]. *Chem. Eng. J.*, 2020, 393: 123657.

[140] MING H, ZHANG J F, LIU L L, *et al.*. A novel $Cs_2NbOF_5:Mn^{4+}$ oxyfluoride red phosphor for light-emitting diode devices [J]. *Dalton Trans.*, 2018, 47(45): 16048-16056.

[141] HU M Q, LIU Z F, XIA Y J, *et al.*. The photoluminescence adjustment of red phosphors $ANaWO_2F_4:Mn^{4+}$ (A = Li, Na, K) by suitable tolerance factor designing [J]. *J. Mater. Sci.: Mater. Electron.*, 2020, 31(6): 4535-4541.

[142] LIU Y, LI H, TANG S, *et al.*. A red-emitting phosphor $K_2[MoO_2F_4]\cdot H_2O:Mn^{4+}$ for warm white light-emitting diodes with a high color rendering index [J]. *Mater. Res. Bull.*, 2020, 122: 110675.

[143] JANSEN T, FUNKE L M, GOROBEZ J, *et al.*. Red-emitting $K_3HF_2WO_2F_4:Mn^{4+}$ for application in warm-white phosphor-converted LEDs-optical properties and magnetic resonance characterization [J]. *Dalton Trans.*, 2019, 48(16): 5361-5371.

[144] STOLL C, SEIBALD M, BAUMANN D, *et al.*. HF-free solid-state synthesis of the oxyfluoride phosphor $K_3MoOF_7:Mn^{4+}$ [J]. *Eur. J. Inorg. Chem.*, 2019, 2019(29): 3383-3388.

[145] STOLL C, HEYMANN G, SEIBALD M, *et al.*. $K_3WOF_7:Mn^{4+}$—a red oxyfluoride phosphor [J]. *J. Fluor. Chem.*, 2019, 226: 109356.

[146] KHAIDUKOV N, BREKHOVSKIKH M, TOCI G, *et al.*. Time- and temperature-resolved luminescence spectroscopy of $LiAl_4O_6F$: Mn red phosphors [J]. *J. Lumin.*, 2019, 216: 116754.

[147] SHAO Q Y, LIN H N, HU J L, *et al.*. Temperature-dependent photoluminescence properties of deep-red emitting Mn^{4+}-activated magnesium fluorogermanate phosphors [J]. *J. Alloys Compd.*, 2013, 552: 370-375.

[148] CAI P Q, WANG X F, SEO H J. Excitation power dependent optical temperature behaviors in Mn^{4+} doped oxyfluoride $Na_2WO_2F_4$ [J]. *Phys. Chem. Chem. Phys.*, 2018, 20(3): 2028-2035.

[149] WANG Z L, YANG Z Y, YANG Z F, *et al.*. Red phosphor $Rb_2NbOF_5:Mn^{4+}$ for warm white light-emitting diodes with a high color-rendering index [J]. *Inorg. Chem.*, 2019, 58(1) 456-461.

[150] KATO H, TAKEDA Y, KOBAYASHI M, *et al.*. Photoluminescence properties of layered perovskite-type strontium scandium oxyfluoride activated with Mn^{4+} [J]. *Front. Chem.*, 2018, 6: 467.

[151] MA C G, WANG Y, LIU D X, *et al.*. Origin of the β_1 parameter describing the nephelauxetic effect in transition metal ions with spin-forbidden emissions [J]. *J. Lumin.*, 2018, 197: 142-146.

[152] BRIK M G, BEERS W W, COHEN W, *et al.*. On the Mn^{4+} R-line emission intensity and its tunability in solids [J]. *Opt. Mater.*, 2019, 91: 338-343.

[153] SRIVASTAVA A M, BRIK M G, COMANZO H A, *et al.*. Spectroscopy of Mn^{4+} in double perovskites, La_2LiSbO_6 and La_2MgTiO_6: deep red photon generators for agriculture LEDs [J]. *ECS J. Sol. State Sci. Technol.*, 2018, 7(1): R3158-R3162.

[154] LIU D X, MA C G, HU P W, *et al*.. First-principles and crystal-field calculations of the electronic and optical properties of two novel red phosphors $Rb_2HfF_6:Mn^{4+}$ and $Cs_2HfF_6:Mn^{4+}$ [J]. *J. Am. Ceram. Soc.*, 2018, 101(6): 2368-2375.

[155] WANG Z L, YANG Z Y, WANG N, *et al*.. Single-crystal red phosphors: enhanced optical efficiency and improved chemical stability for wLEDs [J]. *Adv. Opt. Mater.*, 2020, 8(6): 1901512.

BRIK Mikhail G (1969 –), received his PhD from Kuban State University (Russia) in 1995 and his DSc (habilitation) from the Institute of Physics, Polish Academy of Sciences (Poland) in 2012. Since 2007 he is a professor at the Institute of Physics, University of Tartu, Estonia. Before that, he worked at Kyoto University (Japan) from 2003 to 2007, Weizmann Institute of Science (Israel) in 2002, Asmara University (Eritrea) from 2000 to 2001, and Kuban State University from 1995 to 2000. He is also a distinguished visiting professor at Chongqing University of Posts and Telecommunications (China) and Professor at Jan Długosz University (Poland). Since 2015 he serves as one of the editors of *Optical Materials* (Elsevier). Professor Brik's scientific interests cover theoretical spectroscopy of transition metal and rare earth ions in optical materials, crystal field theory, and ab initio calculations of the physical properties of pure and doped functional compounds. He is a coeditor of two books and author of 12 book chapters and about 410 papers in international journals. According to Google Scholar (June 2020), he has more than 8 500 citations with H index 45. He received the Dragomir Hurmuzescu Award of Romanian Academy in 2006 and the State Prize of the Republic of Estonia in the field of exact sciences in 2013. In 2018 he received the state professor title from the President of Poland.

E-mail: mikhail. brik@ ut. ee

MA Chong-geng (1980 –), received his PhD from University of Science and Technology of China in 2008. He spent three years (2010—2013) as a post-doctor in University of Tartu with the financial support of European Social Fund. He was also a visiting professor at University of Verona in 2017. His area of scientific interests covers the first-principles and crystal-field design of luminescent materials. He has published one book and more than 80 papers in international journals, which attracted more than 1 600 citations (H index = 21). Currently he is a full professor and the director of CQUPT-BUL Innovation Institute at Chongqing University of Posts and Telecommunications.

E-mail: macg@ cqupt. edu. cn

SRIVASTAVA Alok M (1960 –), received his PhD from in 1986 from Polytechnic University of New York, Brooklyn, New York. Dr. Srivastava began his industrial career at General Electric's (GE) Global Research Center in Niskayuna, New York, in 1989 at GE GRC he established the phosphor laboratory where he laid the groundwork for the design and development of luminescent materials. Dr. Srivastava's research describes the relationship between the synthesis, crystal structure and optical properties of luminescent ions in solids. Dr. Srivastava holds a total of 141 U. S. patents and more than 100 peer reviewed publications. In 2015 he was appointed the Editor-in-Chief of Journal of Optical Materials (Elsevier). For his pioneering research in oxide quantum splitting phosphors he was awarded the First Centennial Outstanding Achievement Award of the Luminescence and Display Materials Division of The Electrochemical Society (2004). He has served as the Chairman of the Luminescence and Display Materials group of The Electrochemical Society. In 2019, Dr. Srivastava was elected Fellow of The Electrochemical Society. Currently, Dr. Srivastava has a technical consulting firm that is based on his more than 35 years of experience and broad technical knowledge in the area of solid-state luminescence. He leverages his expertise to assist industrial and academic scientists in the fundamental understanding, design and synthesis of luminescent products.

E-mail: srivastaam@ outlook. com

PIASECKI Michal (1957 –), received his MSc in Physics (honors degree) in Institute of Physics, Nicolaus Copernicus University Torun (present A. Jablonski Institute), Ph. D. from Institute of Low Temperature and Structural Research Polish Academy of Sciences in Wroclaw (Poland) and habilitation in Zielona Gora University (Poland). Now he is working as a professor and Head of Department of Theoretical Physics of Jan Długosz University (Poland) and Lesya Ukrainka Eastern European National University (Ukraine). His research interests cover phase transitions, ferroelectricity, thermoelectricity, luminescence and non-linear optics. He conducted several EU projects utilizing ultra-UV (synchrotron) spectroscopic ellipsometry for investigations of novel photonic materials and bilateral research projects between Poland and France, Portugal, *etc* as partner countries. He has more than 170 publications in SCI journals, H-index = 22, more than 1 900 citations. He has several awards including those from Polish Academy of Sciences – 2 times; Polish Ministry of Sciences and Higher Education; Rector of Jan Długosz University. He was a visiting professor in University of Reims Champagne-Ardenne (France) and Vellore Institute of Technology, India.

E-mail: m. piasecki@ ujd. edu. pl